Applications of LRB and FPS to 3-D Curved Box Bridges

Ying-Hui Lei* and Yu-Lin Chien

Department of Civil Engineering
Tamkang University
Tamsui,Taiwan 251, R.O.C.
E-mail: demanad@mail.tku.edu.tw

Abstract

Although, compared to the use of the conventional straight bridge, the adoption of the curved bridge will usually take higher price in construction and more sophisticated thinking in designing, this type of structures are, however, met frequently at freeway interchanges or some spots under changeable terrain. Even subjected to the seismic force acting along a fixed direction, nonlinear isolators installed in the curved bridge would move in an extremely unpredicted way. Accordingly, the proper description for the relationship between force and displacement of the isolator hence becomes a crucial work to do. In this research, the effective analytical scheme for estimating the stressed conditions of isolators including both lead rubber bearing (L.R.B.) and friction pendulum system (F.P.S.) will be established first, and then the dynamic behavior of a series of isolated curved bridges subjected to the earthquake either with a typical low-frequency or high-frequency content of acceleration will be investigated in detail afterward. It is shown in the results that isolation performance on base shear reduction will be closely related to the content of earthquake and the curvature angle of structure.

***Key Word*:** Curved Bridges, Isolation Effects, LRB, FPS, Content of Acceleration

1. Introduction

Being suitable for the local transportation needs and particular terrain conditions, the curved bridge has become one of the most significant structures in the modern transportation construction. Since the effectiveness of isolation elements in protecting the straight bridge under earthquake loading has been comprehensively recognized, the investigation of seismic behaviors for the isolated curved bridge would thus not only be rich in theoretical challenge but also be crucial in practice. Seismic analysis with respect to the straight bridge installed with isolators behaving in nonlinearity and being subjected to a ground excitation acting in a direction not parallel or perpendicular to the longitudinal axis of the deck would become quite cumbersome since each point of the straight bridge considered might exhibit a fairly irregular 2-D motion. The complicacy involved would be even more profound if the straight bridge is replaced by the structure of curved bridge. This is because the coupling effect of bending moment and rotational torque would always be induced to the curved bridge due to the geometric nature of itself. Therefore, the difficulties that will be confronted in seismic analysis of the isolated curved bridge will contain how to determine the precise moving trajectories and how to obtain the correct stress conditions of the isolator concerned.

The finite element technique, with the employment of a great number of straight beam elements spreading densely over the structure, is frequently to be used for acquiring the approximate solution of the curved bridge. This approach,

however, would accompany some significant drawbacks such as the high computational cost as well as the incapability of taking warping effects into account. Consequently, some of the researchers have devoted themselves to develop effective curved beam elements so as to replace the use of conventional straight beam elements. In the early age, relevant study was primarily focused upon the curved elements incapable of taking the transverse load effects into account [1−3]. In 1992, Kou, Benzley and Huang proposed a 3-D curved thin-walled beam element with seven degrees of freedom at each node, in which one of the degrees of freedom mentioned is used exclusively for describing the warping effects involved [4]. This will also be the type of curved beam elements utilized in the current research for investigating the seismic behaviors of the curved bridge in both isolated and un-isolated cases.

Ever since the successful development of laminated rubber bearings in 1977 [5,6], the concept for applying the isolation system to various patterns of structures for enhancing the structural safety under strong ground motion has been widely accepted by earthquake engineers. The isolator of LRB, installed in William Clayton Building of Wellington city in New Zealand as its first application to an existing structure [7], and the isolator of FPS, proposed and having been undertaken an intensive experiment by the Earthquake Engineering Research Center at University of California in Berkeley [8], will be used in this investigation.

2. Formulation of Curved Thin-walled Beam Elements

Figure 1 illustrates the local coordinate system associated with the formulation of the curved thin-walled beam element, in which x- and y-axes are coincident, respectively, with two principal axes perpendicular each other over the cross section considered, and z-axis is collinear with the tangential line formed by connecting the centroidal points at various sections together. Referring to Figure 2, the internal forces at any point k of the curved member may be expressed as follows [4]:

$$F_{sx} = N_{zj}\sin(\alpha-\varphi) + F_{sx,j}\cos(\alpha-\varphi) \tag{1}$$

$$F_{sy} = F_{sy,j} \tag{2}$$

$$N_z = N_{zj}\cos(\alpha-\varphi) - F_{sx,j}\sin(\alpha-\varphi) \tag{3}$$

$$M_x = (T_{zj} - F_{sy,j}r)\sin(\alpha-\varphi) + M_{xj}\cos(\alpha-\varphi) - F_{sx,j}e\sin(\alpha-\varphi) \tag{4}$$

$$M_y = M_{yj} + F_{sx,j}r\sin(\alpha-\varphi) + N_{zj}r[1-\cos(\alpha-\varphi)] \tag{5}$$

$$T_z = T_{zj}\cos(\alpha-\varphi) + F_{sy,j}r[1-\cos(\alpha-\varphi)] - M_{xj}\sin(\alpha-\varphi) + N_{zj}e\sin(\alpha-\varphi) \tag{6}$$

$$M_\omega = \mu\left\{\eta(T_{yj}r^2 - T_{zj}r)\sin(\alpha-\varphi) - \frac{T_{zj}(1-\eta)+F_{sy,j}r\eta}{k} \cdot\frac{\cos\alpha\sinh k(L-z)}{\cosh kL} - \frac{F_{sy,j}r(1-\cos\alpha)}{k} \cdot\frac{\sinh k(L-z)}{\cosh kL} + (M_{xj}-N_{zj}e)\frac{(1-\eta)\sin\alpha}{k} \cdot\frac{\sinh k(L-z)}{\cosh kL} - (M_{xj}-N_{zj}e)r\eta[\cos(\alpha-\varphi) - \frac{\cosh kz}{\cosh kL}]\right\} + M_{\omega zj}\frac{\cosh kz}{\cosh kL} \tag{7}$$

where F_{sx} and F_{sy} = shear forces about x- and y-axes respectively; e = eccentricity between shear center and centroid of section; κ = decay coefficient for non-uniform torsion; L = length of element; M_x and M_y = bending moments about x- and y-axes respectively; $M_{\omega z}$ = warping force moment; N_Z = axial force; r = radius of curvature; T_Z = total torque; α = angle subtended by curved member; η = dimensionless parameter; φ = angle of rotation; μ_s = warping shear parameter. The stiffness matrix of the thin-walled curved beam element may be obtained by taking the inverse of the flexibility matrix, and the mass matrix of the element can be established on the basis of Newton's second law of motion [8].

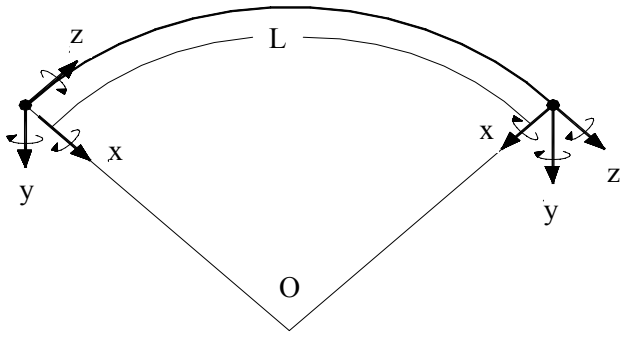

Figure 1. Local coordinates of curved thin-walled beam element.

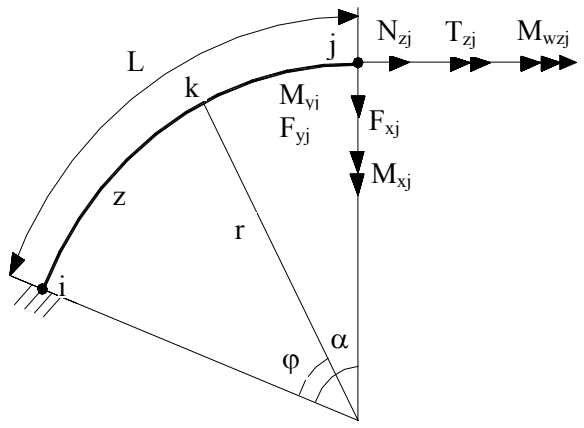

Figure 2. Element forces of curved thin-wall beam element.

3. Effective Modal Mass

The Eqs. of motion for a damped, MDOF system subjected to a ground excitation $\ddot{V}_g(t)$ can always be expressed in matrix notation as

$$M\ddot{V}(t)+C\dot{V}(t)+KV(t)=-S\ddot{V}_g(t)=P_{eff}(t) \tag{8}$$

It can be seen that the distribution of the effective seismic force $P_{eff}(t)$ is dependent upon the spatial distribution vector S given by

$$S=M\{1\}=\sum_{n=1}^{N}S_n \tag{9}$$

In the above Eq. (1) is the quasistatic displacement vector, N is the number of degrees of freedom used for the modeling the system, and S_n is the modal component of S, defined as

$$S_n=\Gamma_n M\Phi_n \tag{10}$$

in which Φ_n is mode shape vector and Γ_n is known as the modal participation factor. Substituting Eq. (10) into Eq. (9) and applying the relations of orthogonality leads to

$$\Gamma_n=\frac{\Phi_n^T S_n}{M_n} \tag{11}$$

in which M_n is generalized modal mass. If C is a classical damping matrix then, with the designation of $q_n(t)$ as modal coordinate, the uncoupled equations of motion can be easily derived to be

$$\ddot{q}_n(t)+2\xi_n\omega_n q_n(t)+\omega_n^2 q_n(t)=-\Gamma_n V_g(t) \tag{12}$$

Evidently, the stiffness force associated with the nth mode caused by $P_{eff}(t)$ will be the product of stiffness matrix K and modal displacement response vector $V_n(t)$, that is

$$f_n(t)=KV_n(t)=S_n\left[\omega_n^2 D_n(t)\right] \tag{13}$$

in which

$$V_n(t)=\Phi_n q_n(t) \tag{14}$$

$$D_n(t)=\frac{q_n(t)}{\Gamma_n} \tag{15}$$

Consequently, the maximum stiffness force corresponding to mode n would be

$$\left|f_n(t)\right|_{\max}=S_n\left(\omega_n^2 S_{dn}\right)=S_n\left(S_{pa,n}\right) \tag{16}$$

in which S_{dn} and $S_{pa,n}$ are spectral displacement and spectral pseudo-acceleration respectively.

According to the relation of Eq. (16), the maximum dynamic response contributed by the nth mode of the system will equal to the product of the modal static response caused by force S_n (having a unit of mass) and the dynamic factor $S_{pa,n}$ (having a unit of acceleration). Therefore, the maximum base shear contributed by mode n with respect to the structure modeled as a shear building as shown in Figure 3 can be expressed as

$$\left|V_{bn}(t)\right|_{\max}=V_{bn}^{st}\left(S_{pa,n}\right) \tag{17}$$

in which V_{bn}^{st} is the modal static response of base shear due to S_n. Designating an alternative name, called as effective modal mass, as well as an alternative notation denoted as M_n^*, to V_{bn}^{st} gives

$$\left|V_{bn}^{st}\right|=\sum_{j=1}^{N}S_{jn}\equiv M_n^* \tag{18}$$

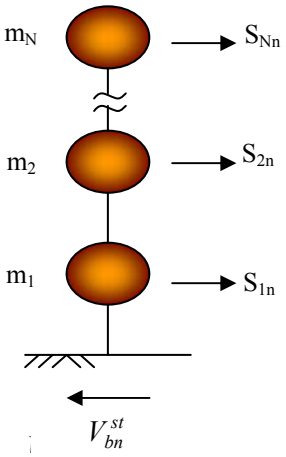

Figure 3. Simple MDOF model for computing V_{bn}^{st}.

Making use of Eqs. (9), (10) and (11) yields

$$M_n^* = \sum_{j=1}^{N} \Gamma_n m_j \phi_{jn} = \frac{\sum_{j=1}^{N} \left(m_j \phi_{jn}\right)^2}{M_n} \tag{19}$$

In order to measure the importance of effective modal mass associated with any mode n, E_{mm} is defined as the modal mass percentage given by

$$E_{mm}(\%) = \frac{M_n^*}{\sum_{j=1}^{N} M_j^*} \times 100 \tag{20}$$

Since M_n^* and $\sum_{i=1}^{n} M_n^*$ are modal static responses of base shear caused by static nodal forces S_n and S respectively, one can thus obtain, by making use of Eq. (9), the following relation:

$$\sum_{j=1}^{N} M_j^* = \sum_{j=1}^{N} m_j \tag{21}$$

As a result, Eq. (20) may be written in an alternative form:

$$E_{mm}(\%) = \frac{M_n^*}{\sum_{j=1}^{N} m_j} \times 100 \tag{22}$$

Following the same derivation procedure as stated above, the maximum modal base shear and the percentage of effective modal mass resulting from the seismic force acting in the direction of, for example, the X-axis of global coordinates (referring to Figure 11) for the structure modeled by any combination of translational and rotational degrees of freedom can thus be expressed separately as

$$\left|V_{bn,x}(t)\right|_{\max} = M_{nx}^* S_{pa,n} \tag{23}$$

$$E_{mm,x}(\%) = \frac{M_{nx}^*}{\sum_{j=1}^{N_x} m_{jx}} \times 100 \tag{24}$$

in which

$$M_{nx}^* = \frac{\left(\sum_{j=1}^{N_x} m_{jx} \phi_{jn,x}\right)^2}{M_n} \tag{25}$$

N_x is number of translational degrees of freedom in X-direction, m_{jx} and $\psi_{jn,x}$ are component elements, associated with X-direction, of lumped mass-matrix and of mode shape vector respectively.

4. Proposed Movable Force Circle

Two types of isolators, known as LRB and FPS, will be installed at the conjunctions of deck and piers of the curved bridge considered. The idealized hysteretic loops used for describing force-displacement relationship of both types of isolators are shown in Figure 4 and 5 respectively, in which k_1 is the lateral stiffness corresponding to initial linear deformation for the isolator of LRB and, as to the isolator of FPS, being the lateral stiffness corresponding to its un-sliding phase, while k_2 is the stiffness corresponding to the subsequent plastic deformation after yielding for the isolator in either LRB or FPS series. Since the isolators considered would move following an extremely irregular path under the ground excitation, it is hence desirable to develop an effective scheme so that the moving trajectories of them, in a form of chaos, can be predicted appropriately. The use of so-called "movable force circle" is introduced herein for this purpose. In accordance with the proposed scheme, each force circle with a radius equal to the yielding force of the isolator, F_y, is considered to consist of two parts, which are the closed circumference line of the force circle and the area inside the circumference line. Whenever the value of isolator stiffness is equal to k_2, the isolator concerned is taken to be in a phase of yielding, while for the cases where isolator stiffness has a value of k_1, the isolator would be regarded as being in a phase of unyielding. The internal force components of the isolator lying in the yielding phase will be obtained in terms of the closed circumference line of movable force circle and in terms of the area inside the circumference line if the isolator is in the unyielding phase. The procedures followed in the applications of the proposed force circle can be summarized as follows:

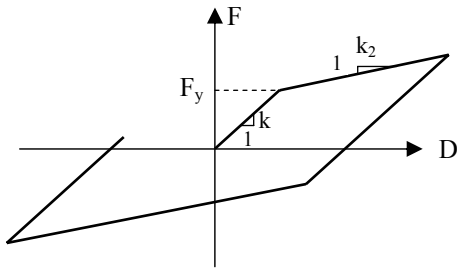

Figure 4. Hysteretic loop of LRB.

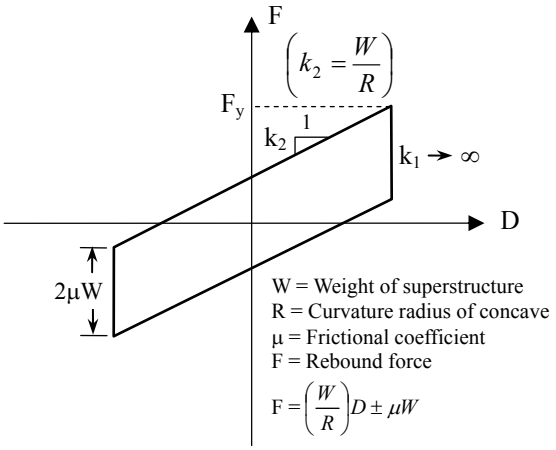

Figure 5. Hysteretic loop of FPS.

(1) Establish a two-dimensional coordinate system with the origin O, the abscissa V_X and the ordinate V_Y used for representing the components of lateral internal force of the isolator in X- and Y-directions respectively, as shown in Figure 6. Before applying of seismic force, the origin of force circle O'_o is set to be coincident with point O.

(2) Calculate V_{Xi} and V_{Yi} at current time t_i, in which the subscript i is denoted as the number of time steps and then mark the point (V_{Xi} , V_{Yi}) on the force circle.

(3) Calculate the distance between the point (V_{Xi} , V_{Yi}) and the origin of the force circle at time t_{i-1}, denoted as O'_{i-1} ($r_{X,i-1}, r_{Y,i-1}$), by using the following equation:

$$V_i^* = \sqrt{(V_{Xi} - r_{X,i-1})^2 + (V_{Yi} - r_{Y,i-1})^2} \tag{26}$$

(4) Determine the location of the origin at time t_i, denoted as O'_i (r_{Xi} , r_{Yi}), by applying the scheme in the following :

(i) If $V_i^* > F_y$ then the isolator will stay in yielding phase, and circle's origin will be shifted to a new location at current time. The coordinates of the origin can be computed by using the equations:

$$r_{Xi} = r_{X,i-1} + \left(V'_{Yi} - F_y \cos\theta\right) \tag{27}$$

$$r_{Yi} = r_{Y,i-1} + \left(V'_{Yi} - F_y \cos\theta\right) \tag{28}$$

in which V'_{xi}, V'_{yi} and θ are given, respectively, by

$$V'_{Xi} = V_{Xi} - r_{X,i-1} \tag{29}$$

$$V'_{Yi} = V_{Yi} - r'_{Y,i-1} \tag{30}$$

$$\theta = \tan^{-1}\left(\frac{V'_{Yi}}{V'_{Xi}}\right) \tag{31}$$

(ii) If $V_i^* \leqq F_y$ then the force circle corresponding to time t_i would be exactly the same as that corresponding to time t_{i-1}. Moreover, the isolator would keep unchangeable in the unyielding phase at current time.

(5) Proceed to time t_{i+1}, and repeat the sequence of calculations from (2) to (4) until the earthquake duration has been experienced.

The determination of the force circles correspond to the movement of the isolator along a prescribed path a → b → c → d → e → f → g → h is illustrated in Figure 6. It is observed that stressed conditions represented by points a, b, e, h would be associated with the unyielding phase whereas those represented by points c, d, f, g would be associated with the yielding phase. To facilitate the application of the proposed force circle, a flowchart is presented in Figure 7.

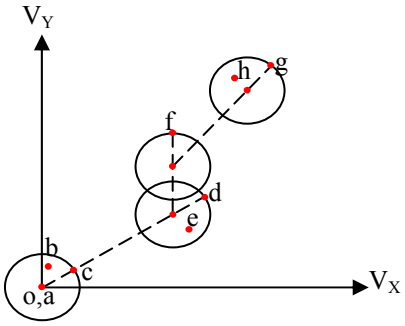

Figure 6. Description for the determination of movable force circle.

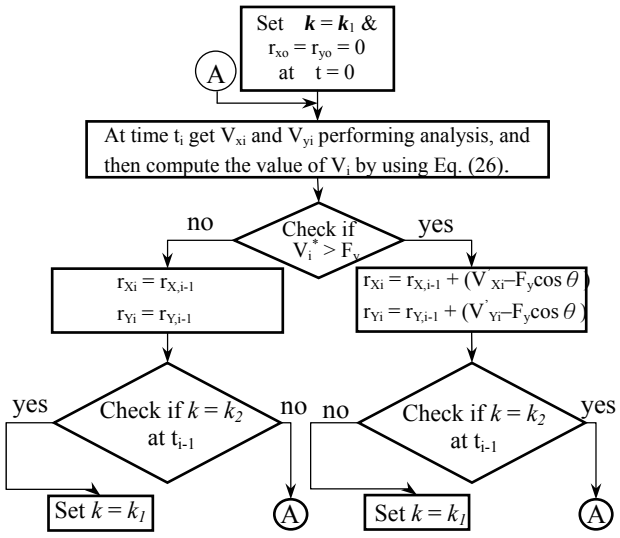

Figure 7. Flowchart for estimating the stressed conditions of isolator.

It is worth mentioning here that describing the stress conditions of the isolator by using a movable force circle but not a movable displacement circle having a radius of yielding displacement of the isolator is mainly due to that the isolators in FPS series having been adopted in the current investigation for earthquake resistance. During un-sliding phase, varied internal forces of FPS would usually correspond to a unique lateral displacement hence poor results might be obtained if one attempts to estimate the stressed conditions of FPS by using a movable displacement circle.

5. Results and Discussion

The curved bridges considered herein would be in a form of three spans and two round piers as sketched in Figure 8, in which a fixed length of span measured along the line created by connecting the centroidal points at various sections of the deck is chosen to be 78.54 m, and each pier will be 10.0 m height and 1.8 m in diameter. Figure 9 shows the cross section of box girders adopted and Table 1 specifies the material properties for both deck and piers. The relevant design parameters for each type of isolators are specified in Table 2, in which the isolators of LRB-1, LRB-2 and LRB-3 are classified into LRB series, and those of FPS-1, FPS-2 and FPS-3 are classified into FPS series. Since it is recognized that the performance of seismic force isolation will be closely dependent upon the frequency content of the external seismic force, El Centro earthquake of May 18, 1952 in U.S. and Taipei A05323L earthquake of May 20, 1986 in Taiwan are chosen respectively as the typical high-frequency and low-frequency seismic forces acting on the structures. Pseudo-acceleration response spectra of these two earthquakes are indicated in Figure 10. During the calculations of the numerical examples indicated in the following, peak values of both earthquakes will be adjusted to 30% the gravity acceleration (0.3 g) for comparison purposes.

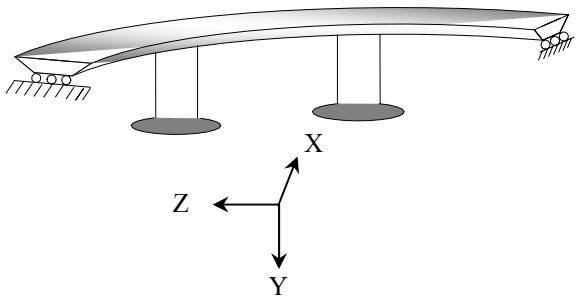

Figure 8. Structural pattern of curved bridge.

Table 1
Material properties of curved bridge

Notation	Box girder	Piers
E (kN/m^2)	2.4525 E07	2.4525 E07
G (kN/m^2)	1.0700 E07	1.0700 E07
A (m^2)	3.929	2.0105
I_x (m^4)	1.4563	0.3217
I_y (m^4)	8.392565	0.3217
J (m^4)	3.47953	0.6434
e (m)	0.06632	--------
μ_s	0.506098	--------

Table 2
Design parameters of LRB and FPS

Notation	LRB-1	LRB-2	LRB-3
K_1 (kN/m)	15696	18639	21582
K_2 (kN/m)	2354	2845	3335
K_y (kN/m)	184.65	277.85	371.30
Notation	**FPS-1**	**FPS-2**	**FPS-3**
R (m)	2.23	2.23	2.23
K_2 (kN/m)	1928	1928	1928
μ	0.03	0.04	0.05
W (kN)	4300	4300	4300
F_y (kN)	172	301	430

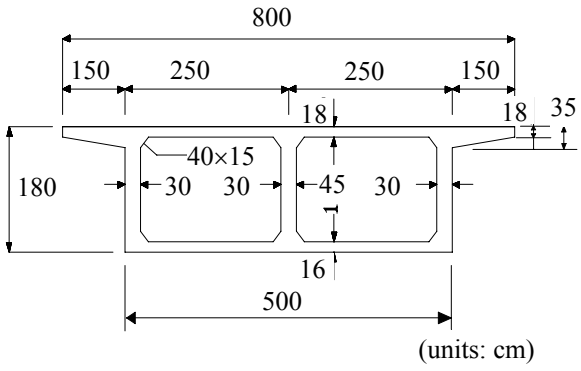

Figure 9. Dimensions of box girder section.

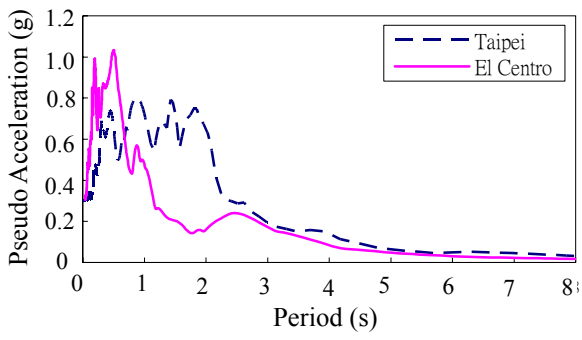

Figure 10. Pseudo-acceleration of two earthquakes.

The analytical model of the isolated curved bridge is shown in Figure 11, in which the direction of X-axis of the global coordinate system is set to be parallel to the symmetric axis of deck plane, and the thin-walled beam element and the 3-D straight beam element will be used for the modeling of the deck and piers respectively. To describe the boundary constraints more realistically, the horizontal movements both in tangential and transverse directions at each end of the deck are assumed to be limited by two elastic springs perpendicular each other. The stiffness of transverse springs, k_l, is taken equal to the initial stiffness k_I of the isolator in LRB series, while the stiffness of tangential springs, k_t, is taken equal to ten times the value of k_l.

The mode shapes corresponding to the first four modes of the curved bridge with an angle of curvature, denoted as β, equal to 90° (referring to Figure 12) under both un-isolated and isolated cases are expressed schematically in Figure 13 and 14. Table 3 specifies the percentage of effective modal mass of the first four modes in X-, Y- and Z-directions respectively for the curved with β = 90° in both isolated and un-isolated cases. It can be seen that as far as the un-isolated cases are concerned, the percentage of effective modal mass would have dominant value in X-direction for the first mode and in Z-direction for the second mode. The variation of these two dominant values with β is indicated in Figure 15. Contrarily, dominant value of the percentage of effective modal mass in isolated cases would be shifted from X-direction to Z-direction for the first mode and from Z-direction to X-direction for the second mode. Moving trajectories in XZ-plane for the isolators of LRB-2 and FPS-2 installed at the conjunction of deck and the left pier of the curved bridge, subjected to the earthquake of El Centro, with β =90° are indicated in Figure 16, in which ξ is defined as the input angle of seismic force, that is the angle measured clockwise in XZ-plane from X-axis to seismic force vector. Quite a chaos motion caused by both types of isolators will be easily found in the sketch.

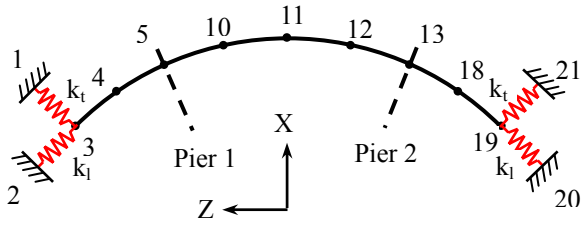

(a) Top view

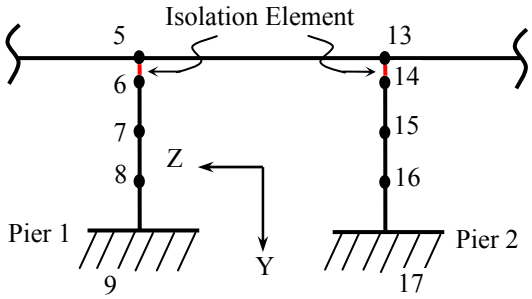

(b) Elevation

Figure 11. Finite-element idealizations of isolated curved bridge.

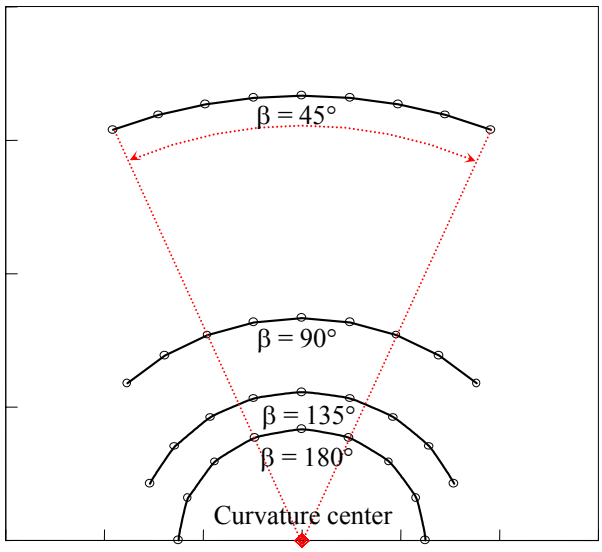

Figure 12. Schematic plot of curved bridges under various angles of curvature.

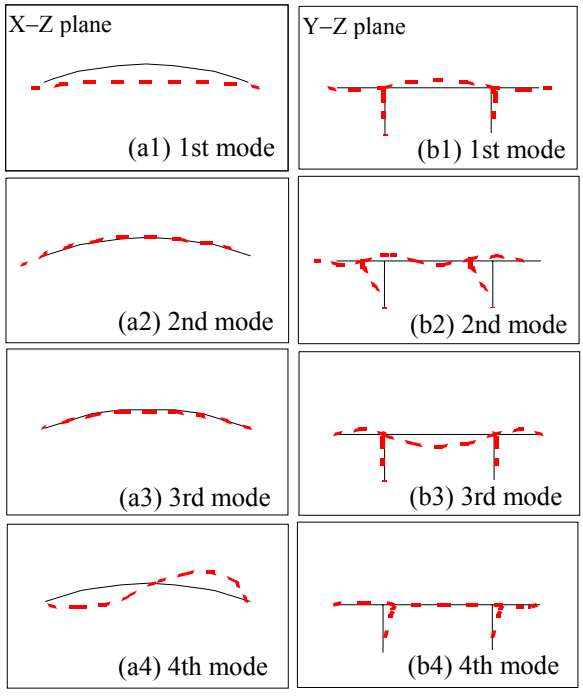

Figure 13. Mode shapes in un-isolated case under $\beta = 90°$.

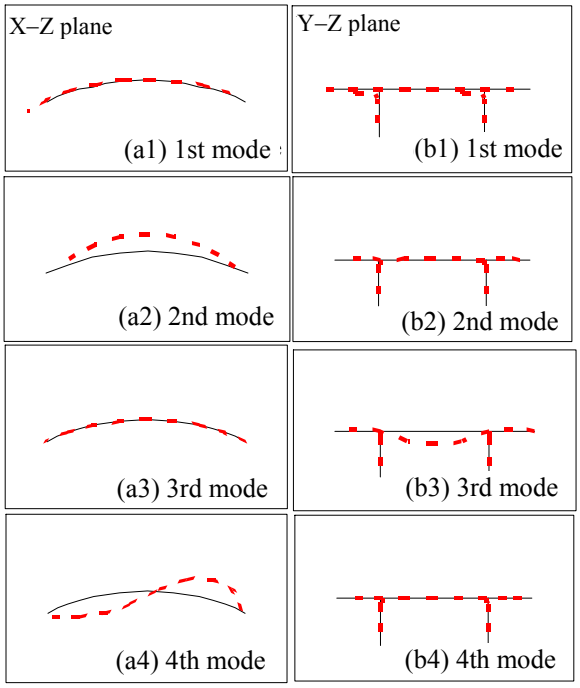

Figure 14. Modal shapes in isolated case under β = 90°.

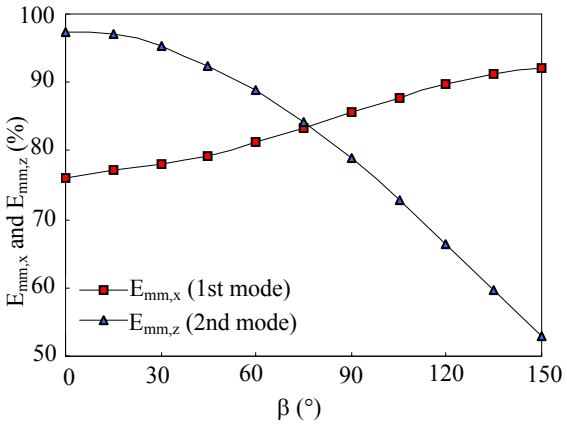

Figure 15. Dominant components of percentage of effective modal mass in un-isolated case.

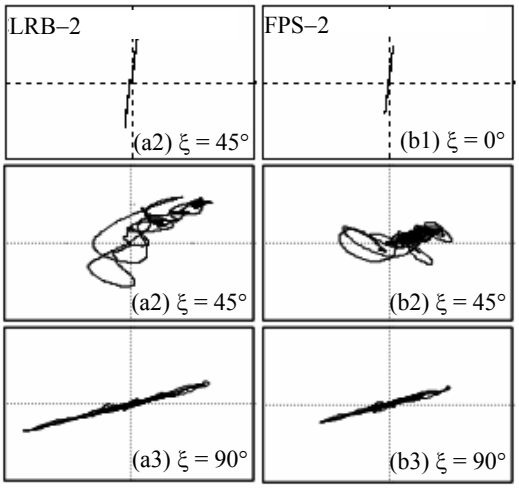

Figure 16. Moving trajectories under β = 90°.

Table 3
Percentage of effective modal mass under $\beta = 90°$

Un-isolated				
Mode	Period (s)	X-dir.	Y-dir.	Z-dir.
1	0.759242	85.5273	0	0
2	0.611926	0	0	78.821
3	0.383471	0	27.3217	0
4	0.269353	0	0	11.0837

FPS-1, FPS-2, FPS-3				
Mode	Period (s)	X-dir.	Y-dir.	Z-dir.
1	0.838781	0	0	78.7664
2	0.752976	86.6858	0	0
3	0.302866	0	36.2146	0
4	0.274152	0	0	11.5176

LRB-1				
Mode	Period (s)	X-dir.	Y-dir.	Z-dir.
1	1.266563	0	0	75.834
2	1.004483	83.6585	0	0
3	0.302755	0	36.1407	0
4	0.284384	0	0	10.966

LRB-2				
Mode	Period (s)	X-dir.	Y-dir.	Z-dir.
1	1.183468	0	0	75.9889
2	0.962107	83.7981	0	0
3	0.302754	0	36.1407	0
4	0.282565	0	0	11.0048

LRB-3				
Mode	Period (s)	X-dir.	Y-dir.	Z-dir.
1	1.118099	0	0	76.1334
2	0.926582	83.9272	0	0
3	0.302754	0	36.1407	0
4	0.280881	0	0	11.0407

Figure 17 and 18 show the variation of the maximum relative displacement for the isolators in LRB series and the variation of the quantity for the isolators in FPS series respectively under the action, in X-direction, of both high-frequency and low-frequency earthquakes, in which the term "relative displacement" is defined as the difference between top and bottom displacements of the isolator considered. It can be observed in these figures that except for a few cases, either higher stiffness of isolators in LRB series or higher frictional coefficient of isolators in FPS series would usually induce a larger relative displacement. Figures 19 and 20 show the variation of the maximum base shear at the left pier for the curved bridge installed with isolators in LRB series, subjected to earthquakes of El Centro and Taipei A05323L, respectively, acting in X-direction, and Figures 21 and 22 show the variation of the quantity for the curved bridge installed with isolators in FPS series under the same earthquakes mentioned respectively. It can be observed that using the isolator with smaller stiffness in LRB series or with lower frictional coefficient in FPS series would induce a better performance on base shear reduction. Furthermore, it can be found that the lines representing the maximum base shear of un-isolated cases in the above figures would vary in a similar way with the lines representing $E_{mm,x}$ of the first mode as shown in Figure 15.

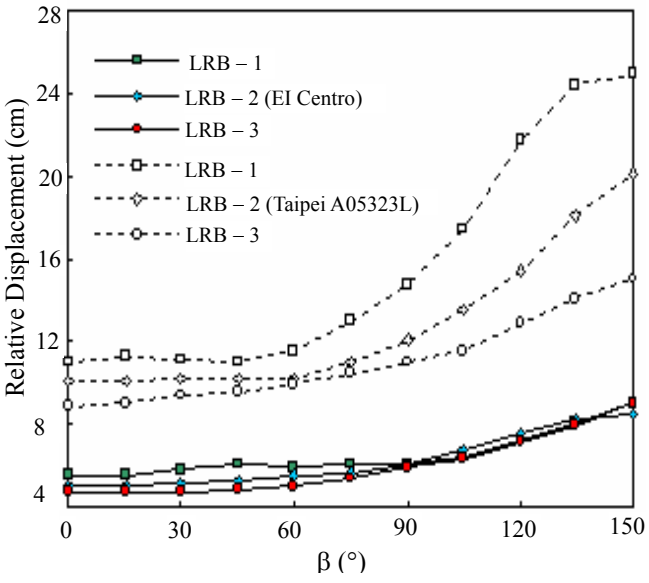

Figure 17. Relative displacement of isolator in LRB series under various earthquakes.

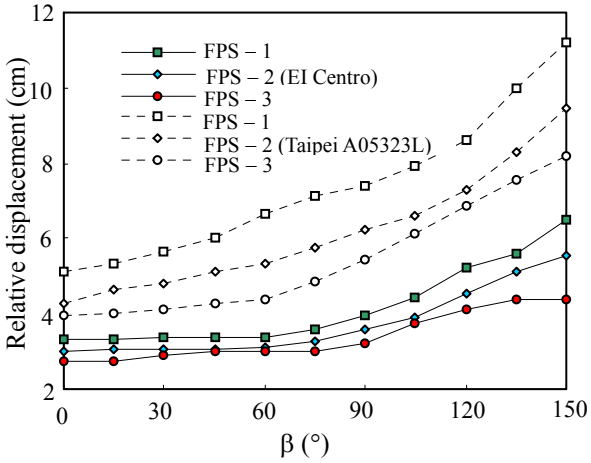

Figure 18. Relative displacement of isolator in FPS series under various earthquakes.

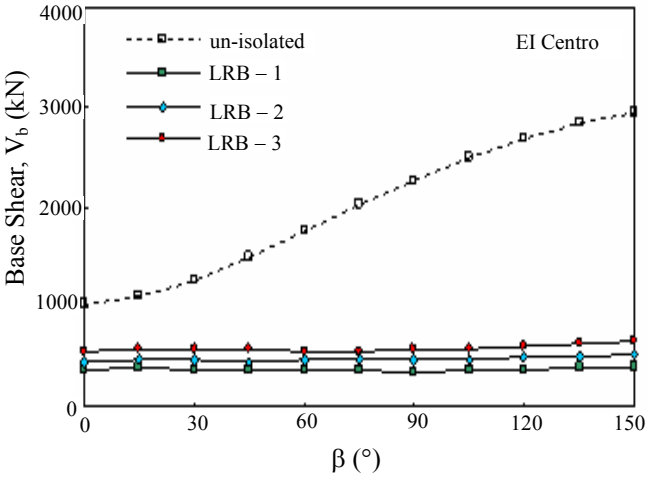

Figure 19. Base shear of curved bridges isolated by LRB and subjected to El centro earthquake.

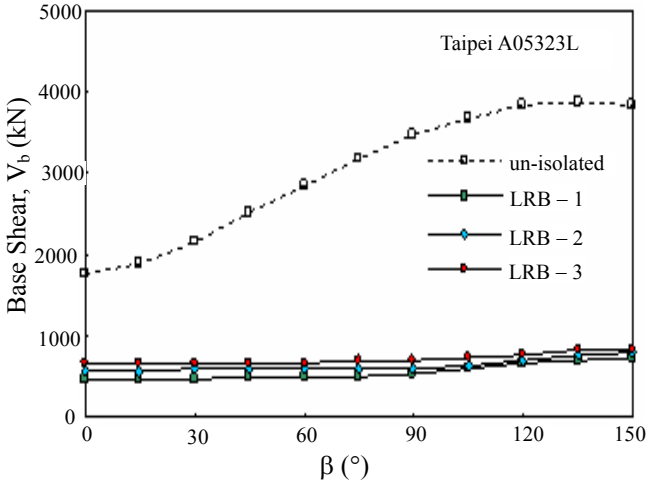

Figure 20. Base shear of curved bridges isolated by LRB and subjected to Taipei A05323L earthquake.

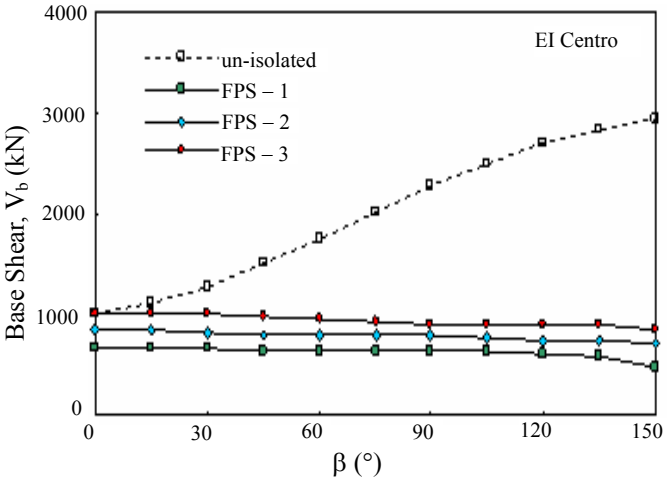

Figure 21. Base shear of curved bridges isolated by FPS and subjected to El centro earthquake.

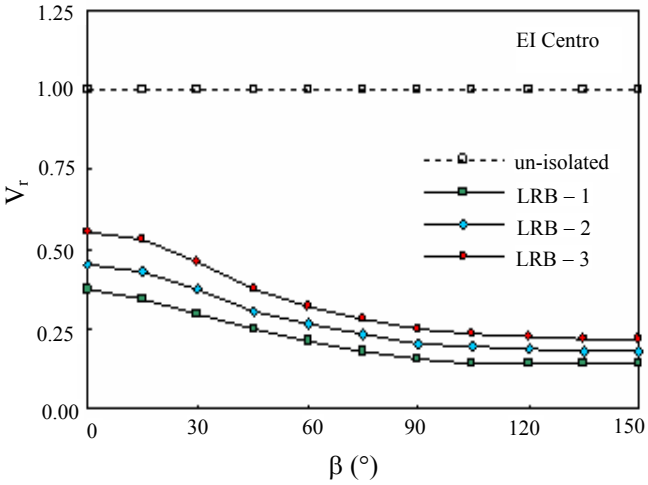

Figure 23. Base shear ratio of curved bridges isolated by LRB and subjected to El centro earthquake.

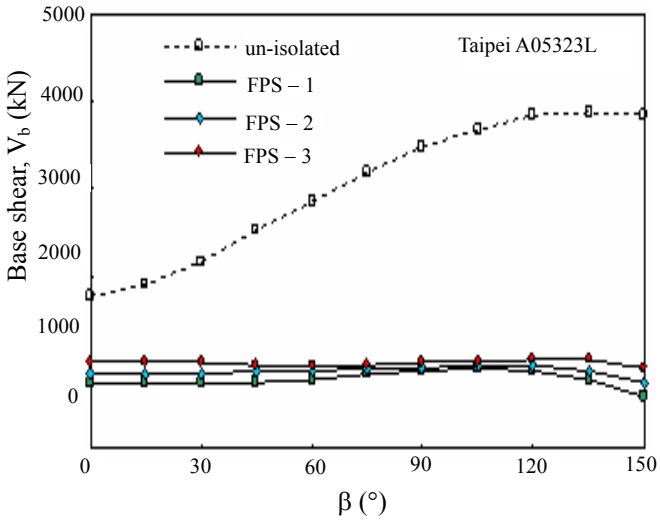

Figure 22. Base shear of curved bridges isolated by LRB and subjected to Taipei A05323L earthquake.

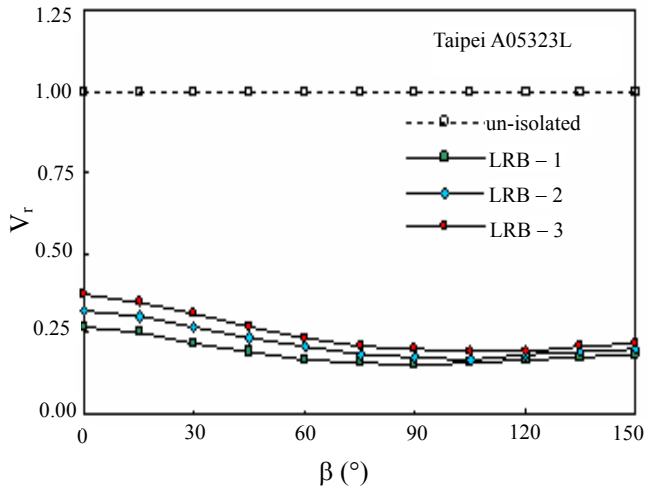

Figure 24. Base shear ratio of curved bridges isolated by LRB and subjected to Taipei A05323L earthquake.

To get a better understanding to the isolation effects of the structure under different circumstances, a series of plots of V_r versus β are shown in Figures 23–26, in which the base shear ratio, V_r, is defined as the ratio of the base shear in any case to that corresponding to un-isolated case, that is $V_r = V_b/V_{b,un\text{-}isolated}$. According to the definition, one may expect that except for un-isolated cases, in which the value of V_r is kept consistently to be unity, the lower V_r is, the more efficient in seismic force isolation will be the isolator. It is indicated in Figures 23–26 that for a given type of isolators, either in LRB or FPS series, structural base shear would be reduced to a greater extent if the structure considered is subjected to the earthquake characterized by its low-frequency content of acceleration than that characterized by its high-frequency content of acceleration. Since the use of the isolators in LRB or FPS series would result in the decrease on fundamental frequency of the structure, the reduction extent of base shear will thus be more significant for the cases where the structures considered are subjected to an earthquake characterized by its high-frequency content of acceleration than by its low-frequency content of acceleration.

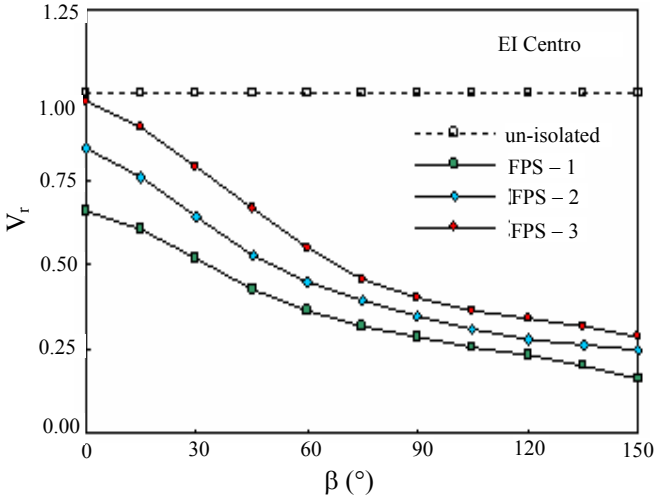

Figure 25. Base shear ratio of curved bridges isolated by FPS and subjected to El centro earthquake.

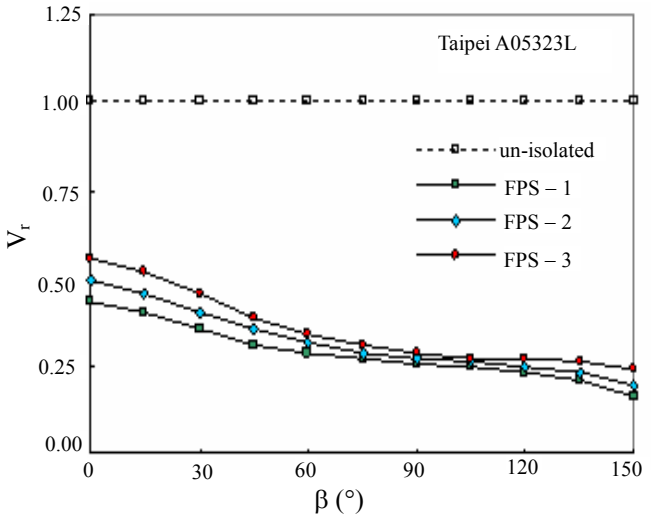

Figure 26. Base shear ratio of curved bridges isolated by FPS subjected to Taipei A05323L earthquake.

6. Conclusion

Owing to the property of material nonlinearity existing in both types of isolators adopted, also owing to the coupling effects of bending moment and rotational torque resulting from the geometric nature of the curved bridge itself, each point of the isolated curved-bridge might exhibit an extremely complicate 2-D motion even though the external disturbance aims at a fixed direction. Consequently, to predict the moving trajectories of isolators properly, a so-called "movable force circle" is introduced herein. With the application of the proposed scheme, some crucial points are observed as follows.

(1) The percentage of effective modal mass can be served as a useful parameter for estimating the importance of modal static base-shear response associated with certain vibration mode shape.

(2) In general, either higher stiffness of isolators in LRB series or higher frictional coefficient of isolators in FPS series would usually induce a larger relative displacement to the isolator itself.

(3) The use of the isolator with smaller stiffness in LRB series or with lower frictional coefficient in FPS series would induce a better performance on base shear reduction.

(4) For a given type of isolators, base shear would be reduced to a greater extent if the structure considered is subjected to an earthquake characterized by its low-frequency content of acceleration than by its high-frequency content of acceleration.

References

[1] Baron, F., "Matrix Analysis of Structures Curved in Space," *Journal of Structural Division*, Vol. 87, ASCE (1961).

[2] Brookhart, G. C., "Circular-arc I-type Girders," *Journal of Structural Division*, Vol. 93, ASCE (1967).

[3] Young, M. C., "Flexibility Influence Foundations for Curved Beams," *Journal of Structural Division*, Vol. 94, ASCE (1969).

[4] Kou, C. H., Benzley, E., Haung, J. Y. and Firmage, D. A, "Free Vibration Analysis of Curved Thin-walled Girder Bridges," *Earthquake Engineering and Structural Dynamics*, Vol. 118, pp. 2890–2910 (1992).

[5] Lee, D. M. and Medland, I. C., "Base Isolation System for Earthquake Protection of Multistory Shear Structure," *Earthquake Engineering and Structural Dynamics*, Vol. 7, pp.555–568 (1979).

[6] Lee, D. M., "Base Isolation for Torsion Reduction in Asymmetric Structure under Earthquake Loading," *Earthquake Engineering and Structural Dynamics*, Vol. 8, pp. 349–359 (1980).

[7] Robinson, W. H., "Lead-rubber Hysteretic Bearings Suitable for Protecting Structures

[8] During Earthquake," *Earthquake Engineering and Structural Dynamics*, Vol. 10, pp. 539–640 (1982).

[9] Zayas, V. A., Low, S. S. and Mahin, S. "Feasibility and Performance Studies on Improving the Earthquake Resistance of Existing Buildings Using the Friction Pendulum System," Earthquake Engineering Research Center, University of California in Berkeley, Report No. EERC-87/01, CA, U.S.A. (1987).

Manuscript Received: Dec. 3, 2003
Accepted: Dec. 31, 2003